Analytical Methods

Deutsche Ausgabe: DOI: 10.1002/ange.201705615
Internationale Ausgabe: DOI: 10.1002/anie.201705615

An Electrochemical Biosensor with Dual Signal Outputs: Toward Simultaneous Quantification of pH and O_2 in the Brain upon Ischemia and in a Tumor during Cancer Starvation Therapy

Li Liu[+], Fan Zhao[+], Wei Liu, Tong Zhu, John Z. H. Zhang, Chen Chen, Zhihui Dai, Huisheng Peng, Jun-Long Huang, Qin Hu, Wenbo Bu, and Yang Tian**

Abstract: *Herein, we develop a novel method for designing electrochemical biosensors with both current and potential signal outputs for the simultaneous determination of two species in a living system. Oxygen (O_2) and pH, simple and very important species, are employed as model molecules. By designing and synthesizing a new molecule, Hemin-aminoferrocene (Hemin-Fc), we create a single electrochemical biosensor for simultaneous detection and ratiometric quantification of O_2 and pH in the brain. The reduction peak current of the hemin group increases with the concentration of O_2 from 1.3 to 200.6 μM. Meanwhile, the peak potential positively shifts with decreasing pH from 8.0 to 5.5, resulting in the simultaneous determination of O_2 and pH. The Fc group can serve as an internal reference for ratiometric biosensing because its current and potential signals remain almost constant with variations of O_2 and pH. The developed biosensor has high temporal and spatial resolutions, as well as remarkable selectivity and accuracy, and is successfully applied in the real-time quantification of O_2 and pH in the brain upon ischemia, as well as in tumor during cancer therapy.*

In vivo analysis of chemical signals in brain extracellular fluid (ECF) using implanted electrochemical biosensors is a vital way to study brain function and brain activity mapping.[1] It offers excellent spatial (10–200 μm) and temporal (ca. s) resolutions and a major advantage of long-term stability. By implanting a microelectrode in a specific brain region, changes in the concentration of a variety of ECF chemical species can be monitored by applying a suitable electrical signal and usually recording the resulting Faradaic current.[2] In this work, a novel method for designing electrochemical biosensors was created. Namely, the molecule Hemin-Fc was designed and synthesized for the simultaneous recognition and real-time quantification of two model molecules, O_2 and pH, during brain ischemia as well as cancer therapy, by monitoring both current and potential signal outputs. Meanwhile, the Fc functional group served as an inner reference, resulting in ratiometric determination with high accuracy.

Both O_2 and pH are critically important species correlated with brain ischemia and cancer growth.[3] During ischemia, when O_2 supply is limited, the electron transport chain of the inner mitochondrial membrane becomes highly reduced. In this reduced state, production of reactive oxygen species (ROS) may result. Then, when respiration is inhibited but glycolysis persists, protons and lactate may be generated, decreasing the pH.[4] On the other hand, both O_2 and pH are vital for cancer growth and the lack of O_2 can lead to hypoxia-induced cell death.[5] However, an analytical method is still the bottleneck for understanding the mechanism of ischemic brain damage, as well as that of cancer growth and death. Over the past decades, many elegant approaches have been established for monitoring of either O_2 or pH.[6] Our group is very interested in the development of biosensors for the detection of ROS, pH, and metal ions in living systems.[3f,7] However, the simultaneous recognition and accurate determination of two of important species such as O_2 and pH is still challenging.

Herein, we designed and synthesized Hemin-Fc, in which a hemin group was connected to two aminoferrocene molecules by an amide bond (Scheme 1a). As demonstrated in Scheme 1b, Hemin-Fc showed two pairs of well-separated electrochemical peaks; one pair located at circa −356 mV vs. Ag/AgCl (half-wave potential $E_{1/2}$) was ascribed to the redox reaction of $Fe^{2+/3+}$ in hemin, the other ($E_{1/2}$) observed at circa 230 mV was attributed to that of Fc. The reduction peak current of $Fe^{2+/3+}$ clearly increased with the increasing concentration of O_2 because of the electrocatalytic activity of the hemin group toward O_2. Interestingly, the $E_{1/2}$ value of $Fe^{2+/3+}$ in Hemin also shifted positively with decreasing pH from 8.0 to 5.5, resulting in simultaneous determination of O_2

[*] L. Liu,[+] F. Zhao,[+] Dr. W. Liu, T. Zhu, Prof. J. Z. H. Zhang, C. Chen, Prof. W. Bu, Prof. Y. Tian
Shanghai Key Laboratory of Green Chemistry and Chemical Processes, School of Chemistry and Molecular Engineering, East China Normal University
Dongchuan Road 500, Shanghai 200241 (China)
E-mail: ytian@chem.ecnu.edu.cn
L. Liu,[+] Prof. Z. Dai
Jiangsu Collaborative Innovation Centre of Biomedical Functional Materials and Jiangsu Key Laboratory of Biofunctional Materials, School of Chemistry and Materials Science, Nanjing Normal University
Nanjing 210023 (China)
Prof. H. Peng
State Key Laboratory of Molecular Engineering of Polymers, Department of Macromolecular Science and Laboratory of Advanced Materials, and Department of Chemistry, Fudan University (China)
J. Huang, Dr. Q. Hu
Discipline of Neuroscience, Department of Anatomy, Histology and Embryology, Shanghai Jiao Tong University School of Medicine Shanghai (China)
[+] These authors contributed equally to this work.
Supporting information and the ORCID identification number(s) for the author(s) of this article can be found under: https://doi.org/10.1002/anie.201705615.

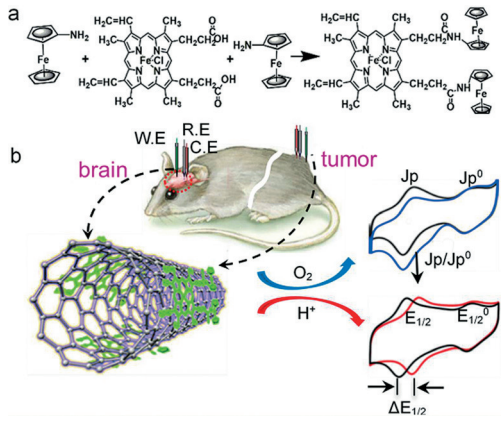

Scheme 1. a) Formation of conjugate Hemin-Fc from hemin and Fc. b) Illustration of working mechanism of the biosensor for simultaneous determination of O_2 and pH.

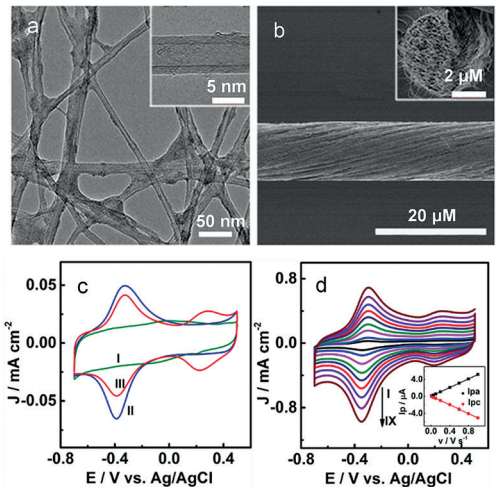

Figure 1. a) TEM images of MWNTs and b) SEM images of CNF. c) Cyclic voltammograms (CVs) obtained in N_2-saturated 0.1 M PBS (pH 7.4), at (I) bare CNF, (II) Hemin/CNF, and (III) Hemin-Fc/CNF microelectrodes. Scan rate = 0.1 $V s^{-1}$. d) CVs obtained at Hemin-Fc/CNF microelectrode in N_2-saturated 0.1 M PBS (pH 7.4) at different scan rates: (I) 0.01, (II) 0.02, (III) 0.05, (IV) 0.1, (V) 0.2, (VI) 0.4, (VII) 0.6, (VIII) 0.8, and (IX) 1.0 $V s^{-1}$. Inset: The linear relationship between peak current intensity of $Fe^{2+/3+}$ in hemin and scan rate.

and pH by monitoring both current and potential signal outputs. Moreover, the Fc group provided a built-in correction for the quantification of O_2 and pH because both peak current and potential of Fc stayed almost constant toward changes of O_2 and pH. Meanwhile, a carbon nanotube fiber (CNF) with a diameter of 10 μm provided a stable and biocompatible substrate for immobilizing Hemin-Fc through π–π stacking. Finally, the developed biosensor was successfully applied for simultaneous detection and accurate quantification of O_2 and pH in live animal brains upon ischemia. The accurate values of O_2 and pH were first reported in different regions of the brain upon ischemia, as well as in tumor during Mg_2Si-starved cancer therapy.

Hemin-Fc was synthesized according to the procedure shown in Scheme 1 a, and its structure was confirmed by mass spectrometry (Figure S1, Supporting Information) and elemental analysis (Table S1). Furthermore, a strong band at 1700 cm^{-1} observed in the IR spectrum of hemin chloride shifts to 1641 cm^{-1} in that of Hemin-Fc (Figure S2, Supporting Information), which was also evidence that the carboxylic group in hemin chloride was successfully converted into an amide group (Scheme 1 a).[8] Multi-walled carbon nanotube (MWNT) fibers were dry-spun from spinnable MWNT arrays at a rotating rate of 2000 rpm, which were synthesized by chemical vapor deposition in advance.[9] The as-prepared MWCNTs are straight and less constrained from the environment (Figure 1 a). The diameter of CNF is circa 10 μm. The end of the MWCNT fiber is abundant with tips of the nanotubes, as seen in Figure 1 b. Hemin-Fc was attached onto the CNF microelectrode through π–π stacking interactions, which was confirmed by UV/vis absorption spectroscopy (Figure S3, Supporting Information).[10] The CNF microelectrode assembled by Hemin-Fc was denoted as Hemin-Fc/CNF microelectrode.

The electrochemical behavior of the Hemin-Fc/CNF microelectrode was then investigated. As shown in Figure 1 c, no obvious redox peak was observed at the bare CNF microelectrode (Curve I), whereas a couple of peaks were obtained at the hemin-modified CNF (denoted as Hemin/CNF) microelectrode (Curve II) with a $E_{1/2}$ value of −356 ± 3 mV, ascribed to the redox reaction of $Fe^{2+/3+}$ at hemin on the CNF microelectrode. For the Hemin-Fc/CNF microelectrode, as expected, two pairs of redox peaks were clearly observed, one pair located at -356 ± 3 mV ($E_{1/2}$) agreed well with the redox reaction of $Fe^{2+/3+}$ in Hemin; the other observed at 230 ± 2 mV was attributed to the Fc group in Hemin-Fc assembled on the CNF microelectrode. Furthermore, both anodic and cathodic peak currents of $Fe^{2+/3+}$ and Fc increased with increasing scan rates, as demonstrated in Figure 1 d, and showed good linearity with scan rates. The result indicates the redox reaction of Hemin-Fc on the CNF microelectrode was a surface-controlled process. The rate constant of the heterogeneous electron transfer (k_s) for hemin on the CNF microelectrode was estimated to be circa 11.83 ± 0.08 s^{-1}, which is much greater than that obtained at the carbon fiber microelectrode-modified MWNT.[11] In addition, the redox responses of the Hemin-Fc/CNF microelectrode demonstrated a negligible change (< 2.7 %) after this electrode was continuously scanned in PBS solution for 1000 cycles (Figure S4 a, Supporting Information), revealing that Hemin-Fc was stably assembled on the CNF microelectrode through π–π stacking interactions. The Hemin-Fc/CNF microelectrode also showed negligible decrease after storage in PBS (pH 7.4) for 7 days (Figure S4 b, Supporting Information). This characteristic is very beneficial for the determination of biological species in complex organisms.

Next, the Hemin-Fc/CNF microelectrode was used for the determination of O_2 and pH. As demonstrated in Figure 2 a, with a rising concentration of O_2, the reduction peak current (J_p) of hemin gradually increased, which resulted from the electrocatalytic activity of hemin to convert O_2 into H_2O through an electrochemical reaction followed by a chemical reaction with one electron and one proton.[12] However, the reduction peak current (J_p^0) for Fc stayed almost constant,

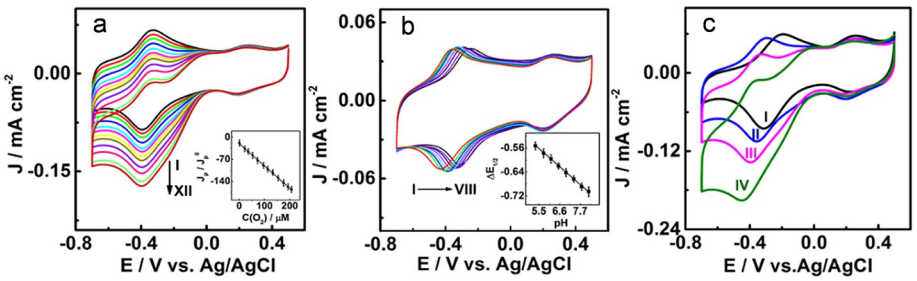

Figure 2. a) CVs obtained at Hemin-Fc/CNF microelectrode in 0.1 M PBS (pH 7.4) bubbled with pure O_2 with different concentrations: (I) 1.3 μM, (II) 21.9 μM, (III) 35.9 μM, (IV) 53.4 μM, (V) 73.1 μM, (VI) 96.2 μM, (VII) 113.1 μM; (VIII) 132.8 μM, (IX) 154.1 μM, (X) 175.6 μM, (XI) 193.1 μM, and (XII) 206.9 μM. Inset: Calibration plot of J_p/J_p^0 against concentration of O_2. b) CVs obtained at Hemin-Fc/CNT microelectrode in 0.1 M PBS (N_2-saturated) with different pH values: (I) 8.14, (II) 7.77, (III) 7.35, (IV) 6.94, (V) 6.54, (VI) 6.14, (VII) 5.75, and (VIII) 5.31. Inset: The calibration plot of $\Delta E_{1/2}$ against different pH. c) CVs obtained at Hemin-Fc/CNT microelectrode in 0.1 M PBS with different pH values and different concentrations of O_2. (I) pH 5.0, $C(O_2) = 1.6$ μM; (II) pH 6.6, $C(O_2) = 83.7$ μM; (III) pH 7.4, $C(O_2) = 132.8$ μM; (IV) pH 8.2, $C(O_2) = 157.5$ μM. Scan rate = 0.1 Vs^{-1}.

leading to the ratiometric determination (J_p/J_p^0) of O_2 with a linear range of 1.3–200.6 μM (inset of Figure 2a). On the other hand, as shown in Figure 2b, $E_{1/2}$ of $Fe^{2+/3+}$ in hemin shifted positively with decreasing pH, while that of Fc had negligible changes. This result allowed us determine pH with good linearity from 5.5 to 8.0 using the potential difference ($\Delta E_{1/2}$) between $E_{1/2}$ of $Fe^{2+/3+}$ and that of Fc. As plotted in inset of Figure 2b, the slope of ΔE versus pH was estimated to be $-55.6\ mV\,pH^{-1}$, indicating a Nernstian process of this redox reaction. More importantly, the Hemin-Fc/CNF biosensor can be applied to the simultaneous detection of O_2 and pH. As shown in Figure 2c, J_p of $Fe^{2+/3+}$ in hemin increased with increasing concentration of O_2 as well as $E_{1/2}$ shifted negatively with increasing pH. Interestingly, neither J_p nor $E_{1/2}$ of Fc showed obvious changes toward the variations of O_2 and pH.

Furthermore, cubic spline interpolation was used to smooth the experimental measurements (Figure S5 & S6, Supporting Information). The resolution of potential, current, and pH are improved to 0.001 V, 0.01 μA, and 0.025, respectively. The calculation was performed using an in-house computer program based on the functions SPLINE and SPLINT.[13] The relational images are summarized in Figure 3, which were employed to quantify the levels of O_2 and pH in the living systems.

Besides accuracy, selectivity is also relatively important for biosensors for use in the brain. The selectivity of the biosensor for simultaneous determination of O_2 and pH was examined against ROS, amino acids, and neurotransmitters. No obvious changes (< 4.8 %) in both peak current and potential of $Fe^{2+/3+}$ were obtained for these biological species (Figure S7, Supporting Information). Meanwhile, negligible changes (< 3.2 %) were observed for the determination of O_2 and pH against the potential interferents. The results indicate high selectivity of the biosensor for the simultaneous determination of O_2 and pH over other biological species that may coexist in living systems.

As demonstrated above, the biosensor shows high temporal and spatial resolutions with remarkable selectivity and accuracy. Thus, it was first applied to the simultaneous determination of O_2 and pH in the brain in vivo. Two ischemic animal models were used; middle cerebral artery occlusion (MCAO)[14] and carotid artery ligation (CAI) (Figure S8, Supporting Information).[15] Figure 4 shows CVs obtained at the Hemin-Fc/CNF microelectrode in the striatum of a normal mouse brain before and after MCAO. It is clear that the reduction peak of $Fe^{2+/3+}$ gradually decreased and peak potential positively shifted with longer MCAO times. After reperfusion, both peak current and potential returned to almost background (Figure 4b). The redox peak of Fc had almost no changes in either current or potential, confirming that Fc can be used as an internal reference. Moreover, the concentrations of O_2, as well as pH values in the cortex, upon MCAO at different times were also investigated (Figure S9, Supporting Information). As demon-

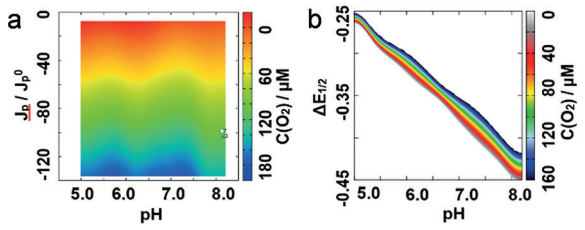

Figure 3. a) Relational graph among J_p/J_p^0, the concentration of O_2, and pH; b) Relational graph among $\Delta E_{1/2}$, the concentration of O_2, and pH.

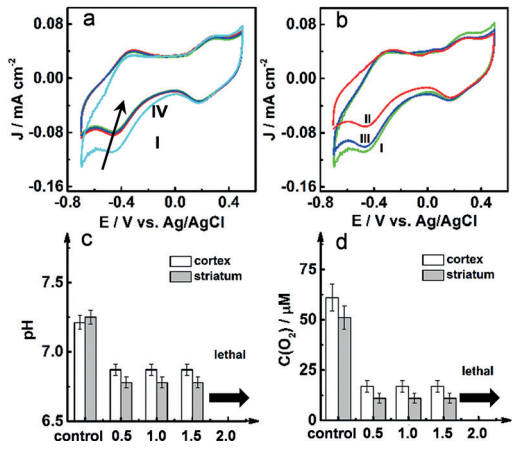

Figure 4. a) CVs obtained at Hemin-Fc/CNF microelectrode in the striatum of (I) normal mouse brain before and after MCAO for (II) 0.5 h, (III) 1 h, and (IV) 1.5 h. b) CVs obtained at Hemin-Fc/CNF microelectrode in the striatum of (I) normal mouse brain before and (II) after MCAO for 1.5 h, and then (III) after reperfusion for 1 h. c) pH values and d) concentrations of O_2 obtained in the cortex and striatum in live mice brain upon MCAO for 0.5, 1.0, 1.5, and 2 h; neuronal cells died after 2 h MCAO.

strated in Figure 4c, pH values of 7.21 ± 0.05 and 7.25 ± 0.05 were observed in the cortex and striatum of normal mouse brain, respectively, which remarkably decreased to 6.87 ± 0.04 and 6.78 ± 0.04 after 1.5 h of MCAO. The initial concentration of O_2 was estimated as 61.0 ± 6.8 and 51.0 ± 5.9 μM in the cortex and striatum (Figure 4d), respectively, and gradually decreased to 17.0 ± 2.8 and 11.0 ± 2.5 μM after 1.5 h of MCAO. As the MCAO time increased to 2 h, neuronal cells died. More interestingly, TTC (2,3,5-triphenyltetrazolium chloride) staining was employed for the fast and reliable visualization of hypoxic and ischemic brain tissue.[16] With the ischemic duration prolonged, the size of cerebral infarction gradually increased (Figure S10, Supporting Information). After MCAO for 2 h, the long-time ischemia induced neuronal death and ischemic brain damage. The present study provided direct evidence that the severity of neuronal death strongly depends on the increased duration of brain acidity that lasts for circa 2.0 h.

Our useful tool was successfully expanded to real-time track O_2 concentrations and pH levels in tumor of live mice after injection of Mg_2Si nanoparticles for cancer starvation therapy (Figure S11–S14, Supporting Information).[17] The initial concentration of O_2 in tumor was estimated as 136.6 ± 9.7 μM and drastically decreased to 53 ± 5.1 μM after injection of Mg_2Si nanoparticles for 1 h. After 2 h, the concentration of O_2 decreased to 4.8 ± 1.3 μM and remained stable even up to 24 h. The pH value in tumor increased sharply from 6.46 ± 0.04 to 7.08 ± 0.05 within 1 h, then gradually increased to 7.18 ± 0.05 after 2 h and maintained a steady state afterwards. Experiments were also carried out in different regions and depths of mouse tumors, which are similar to those demonstrated above. H&E staining assays also showed that after 1 h the tumors starved by the deoxygenation agent feature obvious and significant fibrosis, necrosis, and apoptosis, and such damage became substantially more serious over 24 h (Figure S15, Supporting Information). These results for the first time demonstrated valuable and accurate information on the concentrations of O_2 and pH levels in tumor of live mice upon cancer starvation therapy. This work gave direct evidence that the formation of products from Mg_2Si nanoparticles in the tumor environment blocks blood capillaries and prevents tumors from receiving new supplies of O_2 and nutrients.

A single biosensor for the simultaneous recognition and accurate quantification of O_2 and pH using both current and potential signal outputs with a fast response was developed through the design and synthesis of Hemin-Fc, which was further assembled onto a biocompatible CNF surface with a size of circa10 μm. The redox peak of Fc provided a built-in correction for avoiding environmental effects, leading to a high accuracy. Moreover, the biosensor demonstrated high spatial and temporal resolution, with remarkable selectivity and long-term stability. The biosensor was successfully applied to the simultaneous detection of O_2 and pH in live mouse brains followed by ischemia, as well as in tumor during cancer starvation therapy. The present work has not only provided a new methodology for designing biosensors for the simultaneous determination of multiple species using different signal outputs but has also established a reliable approach for obtaining important information of biological species, which should be very valuable for understanding physiological and pathological pathways of diseases.

Acknowledgements

Support from NSFC (21635003 for Y.T. and 21475062 for Z.D.) and NSFC for Distinguished Young Scholars (21325521 for Y.T. and 21625502 for Z.D.) is acknowledged. The Program of Shanghai Subject Chief Scientist (15XD1501600) is gratefully acknowledged.

Conflict of interest

The authors declare no conflict of interest.

Keywords: analytical methods · brain chemistry · cancer therapy · oxygen · pH

How to cite: *Angew. Chem. Int. Ed.* **2017**, *56*, 10471–10475
Angew. Chem. **2017**, *129*, 10607–10611

[1] a) X. Y. Lang, H. Y. Fu, C. Hou, G. F. Han, P. Yang, Y. B. Liu, Q. Jiang, *Nat. Commun.* **2013**, *10*, 1–4; b) N. V. Kulagina, L. Shankar, A. C. Michael, *Anal. Chem.* **1999**, *71*, 5093–5100; c) T. X. Wei, T. T. Dong, Z. Y. Wang, J. C. Bao, W. W. Tu, Z. H. Dai, *J. Am. Chem. Soc.* **2015**, *137*, 8880–8883.

[2] a) J. Das, I. Ivanov, L. Montermini, J. Rak, E. H. Sargent, S. O. Kelley, *Nat. Chem.* **2015**, *7*, 569–575; b) M. Labib, E. H. Sargent, S. O. Kelley, *Chem. Rev.* **2016**, *116*, 9001–9090; c) S. S. Mahshid, S. Camire, F. Ricci, A. Vallee-Belisle, *J. Am. Chem. Soc.* **2015**, *137*, 15596–15599.

[3] a) J. K. Thompson, M. R. Peterson, R. D. Freeman, *Science* **2003**, *299*, 1070–1072; b) A. E. Ziemann, M. K. Schnizler, G. W. Albert, M. A. Severson, M. A. Howard, M. J. Welsh, J. A. Wemmie, *Nat. Neurosci.* **2008**, *11*, 816–822; c) K. Kaila, *pH and brain function*, Wiley, Hoboken, **1998**; d) E. Taylor, *FEBS Lett.* **1988**, *233*, 216–217; e) O. Ndubuizu, J. C. LaManna, *Antioxid. Redox Signaling* **2007**, *9*, 1207–1219; f) B. Kong, A. Zhu, C. Ding, X. Zhao, B. Li, Y. Tian, *Adv. Mater.* **2012**, *24*, 5844–5848; g) C. Ding, Y. Tian, *Biosens. Bioelectron.* **2015**, *65*, 183–190; h) J. Ma, C. Ding, J. Zhou, Y. Tian, *Biosens. Bioelectron.* **2015**, *70*, 202–208.

[4] a) J. L. Ariansen, M. L. Heien, A. Hermans, P. E. Phillips, I. Hernadi, M. Bermudez, W. Schultz, R. M. Wightman, *Front. Behav. Neurosci.* **2012**, *6*, 36; b) B. J. Venton, D. J. Michael, R. M. Wightman, *J. Neurochem.* **2003**, *84*, 373–381.

[5] C. Zhang, D. Ni, Y. Liu, H. Yao, W. Bu, J. Shi, *Nat. Nanotechnol.* **2017**, *12*, 378–386.

[6] a) D. J. Rossi, J. D. Brady, C. Mohr, *Nat. Neurosci.* **2007**, *10*, 1377–1386; b) L. Xiang, P. Yu, M. Zhang, J. Hao, Y. Wang, L. Zhu, L. Dai, L. Mao, *Anal. Chem.* **2014**, *86*, 5017–5023; c) E. Roussakis, Z. X. Li, A. J. Nichols, C. L. Evans, *Angew. Chem. Int. Ed.* **2015**, *54*, 8340–8362; *Angew. Chem.* **2015**, *127*, 8458–8483; d) J. Zhou, L. M. Zhang, Y. Tian, *Anal. Chem.* **2016**, *88*, 2113–2118; e) F. Zhao, L. Zhang, A. Zhu, G. Shi, Y. Tian, *Chem. Commun.* **2016**, *52*, 3717–3720.

[7] a) B. Kong, A. Zhu, Y. Luo, Y. Tian, Y. Yu, G. Shi, *Angew. Chem. Int. Ed.* **2011**, *50*, 1837–1840; *Angew. Chem.* **2011**, *123*, 1877–1880; b) X. Chai, X. Zhou, A. Zhu, L. Zhang, Y. Qin, G. Shi, Y. Tian, *Angew. Chem. Int. Ed.* **2013**, *52*, 8129; *Angew. Chem.* **2013**,

125, 8287; c) Y. Luo, L. Zhang, W. Liu, Y. Yu, Y. Tian, *Angew. Chem. Int. Ed.* **2015**, *54*, 14053; *Angew. Chem.* **2015**, *127*, 14259.
[8] A. D. Ryabov, V. N. Goral, L. Gorton, E. Csoregi, *Chem. Eur. J.* **1999**, *5*, 961 – 967.
[9] Z. Zhang, K. Guo, Y. Li, X. Li, G. Guan, H. Li, Y. Luo, F. Zhao, Q. Zhang, B. Wei, Q. Pei, H. Peng, *Nat. Photonics* **2015**, *9*, 233 – 238.
[10] Y. X. Xu, L. Zhao, H. Bai, W. J. Hong, C. Li, G. Q. Shi, *J. Am. Chem. Soc.* **2009**, *131*, 13490 – 13497.
[11] D. O. Wipf, E. W. Kristensen, M. R. Deakin, R. M. Wightman, *Anal. Chem.* **1988**, *60*, 306 – 310.
[12] a) Y. Liu, Y. Yan, J. Lei, F. Wu, H. Ju, *Electrochem. Commun.* **2007**, *9*, 2564 – 2570; b) F. Arifuku, K. Mori, T. Muratani, H. Kurihara, *Bull. Chem. Soc. Jpn.* **1992**, *65*, 1491 – 1495.
[13] W. H. Press, S. A. Teukolsky, W. T. Vetterling, B. P. Flannery, *Numerical Recipes in C.*, Cambridge University Press, Cambridge, **1992**.
[14] J. Li, W. Liu, S. Ding, W. Xu, Y. Guan, J. H. Zhang, X. Sun, *Brain Res.* **2008**, *1210*, 223 – 229.
[15] J. Hendrikse, A. F. van Raamt, Y. van der Graaf, W. P. Mali, J. van der Grond, *Radiology* **2005**, *235*, 184 – 189.
[16] Z. Xie, L. Liu, W. Zhu, H. Liu, L. Wang, J. Zhang, C. Chen, H. Zhu, *Artif. Cells Blood Substitutes* **2015**, *43*, 180 – 185.
[17] C. Zhang, D. Ni, Y. Liu, H. Yao, W. Bu, J. Shi, *Nat. Nanotechnol.* **2017**, *12*, 378 – 386.

Manuscript received: June 1, 2017
Revised manuscript received: June 20, 2017
Accepted manuscript online: June 22, 2017
Version of record online: July 24, 2017

